Design and Performance Analysis of MCPC and P4 Waveforms for OFDM based Radar System

Doudou HUANG [1], Jun TANG [2], Longshan XU [1], Yurong WU [1]

[1] Dept. of Materials Science and Engineering, Xiamen University of Technology, Ligong Road 600, 361024 Xiamen, China
[2] Dept. of Opto-Electronic and Communication Engineering, Xiamen University of Technology, Ligong Road 600, 361024 Xiamen, China

hdd0905@outlook.com, jtang@xmut.edu.cn, 15980840308@126.com, yrwu2009@xmut.edu.cn

Submitted September 14, 2023 / Accepted November 24, 2023 / Online first December 18, 2023

Abstract. *This study aimed to investigate the performance of Multicarrier Phase Coding (MCPC) and P4-encoded waveforms. Researchers explored the unique properties of these signals, focusing on aspects like phase distribution, autocorrelation, power spectral density for P4 encoding, and aperiodic autocorrelation and ambiguity function for MCPC signals. The findings identified optimal MCPC sequences with reduced peak-to-mean envelope power ratios (PMEPR), improving signal performance. Complementary codes based on permutation were also generated and analyzed for MCPC sequences. The study utilized an improved genetic algorithm to develop new and improved waveforms, underscoring the importance of techniques like optimal sequence permutation, complementary sequences, and classical window frequency weighting in enhancing signal performance.*

Keywords

MCPC, P4 phase code, autocorrelation function, ambiguity function, improved gene algorithm, classical window frequency weighting

1. Introduction

OFDM (Orthogonal Frequency Division Multiplexing) is a special form of multicarrier modulation (MCM), where individual data streams are generally transmitted on low-rate subcarriers in many cases. Typically, BPSK, QPSK, and other alphabet coding schemes are used to encode and process the information [1]. Existing research on OFDM-based radar communication has been conducted [2–5]. In terms of OFDM waveform design, [3] combines direct sequence spread spectrum (DSSS) and linear modulation (LFM) signals with OFDM for autocorrelation analysis. [4] adds communication data for controlling cyclic shifts to phase-code (PC) OFDM pulses, aiming to investigate radar distance measurement and bit error rate (BER). [5] aims to design OFDM-integrated waveforms that can improve peak-to-average power ratio (PAPR), peak-to-mean envelope power ratio (PMEPR), and peak sidelobe ratio (PSLR). Additionally, a paper [6] proposes an OFDM design scheme based on multicarrier phase coding (MCPC).

MCPC, proposed by Levanon in 2000 [7], is a coding scheme that introduces phase coding based on multicarrier OFDM signals. The purpose of this approach is to achieve balanced performance in terms of spectral efficiency, sidelobe ratio of the ambiguity function, and envelope fluctuations. Current MCPC signals are primarily designed by selecting appropriate weighting factors and phase coding methods on subcarriers to reduce sidelobes of the ambiguity function [8], [9] and control signal envelope fluctuations [10]. However, this method lacks a complete theoretical foundation and requires a large computational burden, making it suitable only for cases with a small number of subcarriers. In the paper [8], the MCPC radar signal simultaneously utilizes N subcarriers, and each subcarrier is phase-modulated by N different sequences that form a complementary set. Each pulse is formed by different periodic frequency shifts of the first pulse, which eliminates the cyclic sidelobes at multiples of the pulse repetition interval but significantly reduces the sidelobe level in the main autocorrelation sidelobes.

Pulse coding, also known as pulse compression, is a signal processing technique aimed at maximizing radar system sensitivity and resolution [11]. It is achieved by modulating the transmitted pulse and then correlating the transmitted pulse with the received signal [12–15]. As a result of the relentless efforts of modern radar signal designers, various PC signals such as Barker codes, Frank codes, P1, P2, P3, P4 and M-sequence codes, as well as frequency-coded signals like Costas signals, have emerged [16–18]. These coding signals have been widely applied in many radar systems, overcoming the need to extend radar operating distance while maintaining the required distance accuracy and solution.

The paper [9] describes a series of MCPC signals based on modulating all subcarriers with the same sequence and applying phase modulation to the subcarriers to reduce PMEPR. The spectral characteristics of the new MCPC signals are

DOI: 10.13164/re.2024.0062

compared with other low PMEPR MCPC signals and single-carrier PC waveforms with the same compression ratio and fixed envelope. To address the issue of reducing PMEPR at the expense of degrading the high sidelobe ambiguity in MCPC radar waveforms designed based on Continuous Orthogonal Complementary Sequences (COCS), Salil Sharma et al, propose a method that utilizes Constant Envelope (CE) modulation and filtering operations to reduce PMEPR [19]. The papers [20], [21] introduce a novel method based on Fast Fourier Transform (FFT), which is mathematically equivalent to matched filtering but offers lower computational complexity compared to traditional methods.

In recent research, it can be observed that [22] proposes a waveform called Interrupted Sample Repeater Jamming (ISRJ) based on MCPC signals. This waveform employs chaotic two-phase encoding on each OFDM signal chip and then extracts the signal by truncating equal-length code chips with different subcarriers. [23–25] present a new method for generating MCPC signals using a direct calculation approach, which offers lower computational complexity.

In the realm of radar-communication integration, several integrated approaches have been suggested. Notably, Donnet and Longstaff endorsed merging MIMO radar with MCPC communication technology [26]. Lellouch and Nikookar from the Netherlands proposed combining MCPC communication tech with radar systems [27]. Additionally, Garmatyuk's team at the University of Miami recommended integrating MCPC communication and radar tech to establish a comprehensive radar-communication system [28]. This study, conducted in the context of MCPC radar signals, aims to address the limitations of traditional radar systems that employ single-frequency continuous-wave or pulse signals, resulting in restricted range resolution and vulnerability to multipath interference and noise. To enhance radar performance, we advocate the use of MCPC radar signals. The study involves assessing the performance of MCPC OFDM waveforms encoded with P4, optimizing sequence orders, and employing an enhanced genetic algorithm to reduce the PMEPR value.

The organizational structure of the remaining sections of this paper is delineated as follows. Section 2 is dedicated to the establishment of the corresponding OFDM signal model, encompassing the computation of P4 phase encoding sequences and the analysis of autocorrelation functions. In Sec. 3, an amalgamation of these components results in the development of an OFDM signal model employing P4 encoding modulation. Section 4 provides an exposition of the comprehensive utilization of P4 in all cyclic shifts within the context of MCPC. Section 5 undertakes a numerical analysis of complementary MCPC pulse sequences based on the aforementioned, and through the application of an enhanced genetic algorithm, derives optimized waveforms with lower PMEPR values. Lastly, Section 6 serves as a culmination, offering a comprehensive summary of the content presented throughout this document.

2. OFDM Signal and P4 Code

2.1 OFDM Signal Process Model

The use of multi-carrier modulation enables high-speed data transmission, effectively mitigating the impact of frequency selective fading, alleviating multipath effects, and enabling independent equalization processing. This approach overcomes the limitations of single-carrier transmission in broadband channels, thereby improving reliability and performance. At the transmitter, the wideband signal resources. To address this, narrowband filtering is employed to selectively pass signals within specific frequency ranges while suppressing others. This process decomposes the original wideband signal into multiple non-overlapping narrowband signals [29]. The general form of an OFDM signal can be represented as follows:

$$s(t) = \sum_{m=1}^{N} \omega_n \exp(\mathrm{j}2\pi\Delta f t)\, u_n(t/T_\mathrm{b}) \tag{1}$$

where N represents the number of subcarriers, ω_n denotes the weighting coefficient of the N-th subcarrier, T_b represents the duration of an OFDM symbol, $u_n(t/T_\mathrm{b})$ represents the rectangular envelope of the data for the N-th subcarrier, Δf represents the frequency spacing between subcarriers and $T\Delta f = 1$.

From the above, it can be observed that the complete waveform of the OFDM signal is formed by the linear superposition of multiple independent frequency components in the time domain. The OFDM signal consists of N subcarriers, each with its own frequency component, and this subcarrier's data is modulated using a rectangular envelope, resulting in the independent frequency components that contribute to the overall OFDM signal.

In the frequency domain, each subcarrier is represented as a narrowband signal with a frequency of f_i. When two subcarriers have different frequencies, they are independent of each other in the frequency domain, and can thus be expressed as:

$$\begin{aligned}
\langle s_1(t), s_2(t)\rangle &= \int_{-\infty}^{\infty} s_1(t)\, s_2^*(t)\,\mathrm{d}t \\
&= \int_{-\infty}^{\infty} \sum_{n_1=0}^{N-1} A_{1,n_1} \exp(\mathrm{j}2\pi n_1 f_1 t) \\
&\quad \sum_{n_2=0}^{N-1} A_{2,n_2}^* \exp(-\mathrm{j}2\pi n_2 f_2 t)\,\mathrm{d}t \\
&= \sum_{n_1=0}^{N-1}\sum_{n_2=0}^{N-1} A_{1,n_1} A_{2,n_2}^* \\
&\quad \int_{-\infty}^{\infty} \exp[\mathrm{j}2\pi(n_1 f_1 - n_2 f_2)\, t]\mathrm{d}t \\
&= \sum_{n_1=0}^{N-1}\sum_{n_2=0}^{N-1} A_{1,n_1} A_{2,n_2}^* \delta(n_1 - n_2) \\
&= \begin{cases} 0, & n_1 \neq n_2 \\ 1, & n_1 = n_2 \end{cases}
\end{aligned} \tag{2}$$

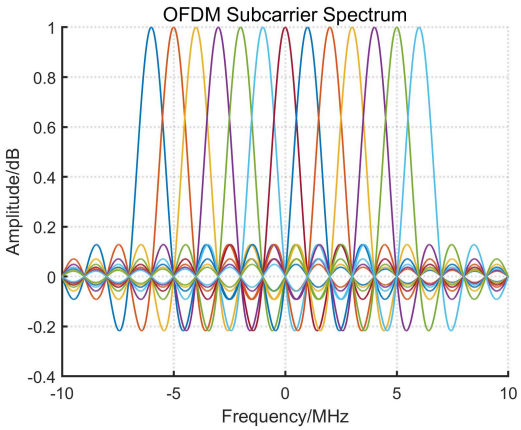

Fig. 1. Frequency spectrum of OFDM subcarriers.

where $\delta(n)$ represented the Dirac function. However, when two subcarriers have the same frequency, they exhibit an overlapping region in the frequency domain. In such cases, the Dirac impulse function is used to calculate their temporal inner product, ensuring that different subcarriers satisfy the orthogonality condition.

In an OFDM system, each subcarrier sequence transmits its signal through overlapping with each other, which is then combined into a composite signal $f(t)$ at the receiver. The receiver performs multiplication and integration operations on the composite signal $f(t)$ to extract the individual signals carried by each subcarrier.

According to frequency domain analysis, the time-domain multiplication in $s(t)$ corresponds to convolution in the frequency domain. The frequency spectrum amplitude of a commonly used rectangular pulse is given by the sinc (fT) function, where the maximum value is located at $f = 0$ and is zeros at frequency points of $n/T, n \in Z$. This is illustrated in Fig. 1, depicting the frequency spectrum of OFDM subcarriers. During demodulation, by calculating the maximum value of each subcarrier's frequency spectrum, it can be determined that only the subcarriers at those maximum value points carry signals. By aligning the maximum value points, symbols from each overlapping subchannel can be extracted without interference from other overlapping subchannels [30].

2.2 P4 Polyphase Code

P4 code is widely used in the field of digital communication and is suitable for various data transmission scenarios, including serial communication, sensor data transmission, industrial automation, data communication network, and so on. In the P4 code, the real and imaginary parts of the baseband linear LFM signal are individually subjected to Nyquist sampling, resulting in discrete sequences of the real and imaginary parts. These sequences undergo encoding and can be used for transmission or storage, and can be decoded at the receiver to reconstruct the original baseband linear frequency modulation signal. The local frequency of the LFM signal, ensures that the P4 code has the highest phase increment at the edges of the code, thereby exhibiting good bandwidth-limiting properties. This characteristic facilitates the reduction of out-of-band noise superposition, thereby improving the reliability of transmission [31]. The phase increment of the P4 code is given as:

$$\phi_m = \frac{\pi(m-1)^2}{M} - \pi(M-1) \tag{3}$$

where $m = 1, 2, 3, \cdots, M$, M is the number of code fragments in sequence. The core principle of P4 code lies in coding information through phase variations, combing the advantages of phase modulation and linear modulation to achieve efficient data transmission. By leveraging the phase characteristics of the carrier signal, P4 code provides a robust and reliable method for coding and decoding digital information in communication systems.

By setting the P4 coding length, the sampling time per sample, the data transmission rate, and the total number of samples according to (3), the P4-phase coded sequence is generated. Subsequently, the relevant discrete sequence data is plotted to obtain the P4 coding phase image and the real part waveform, as shown in Figs. 2 and 3. From the figures, it is evident that in the P4 coding sequence, the real part represents the amplitude information of the waveform, while the phase represents the phase information. Due to the periodic nature of the P4 coding sequence, the waveform samples within each period exhibit similar amplitude and phase characteristics. Additionally, the phase undergoes comparable variations within each period, resulting in a pronounced symmetry observed in the P4 coding sequence image.

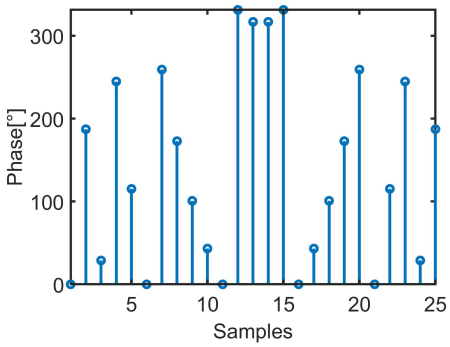

Fig. 2. P4-phase coded sequence.

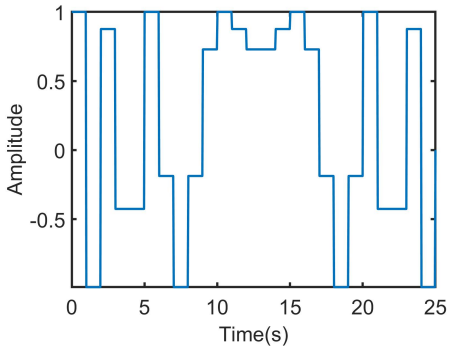

Fig. 3. P4-phase coded sequence real part of waveform.

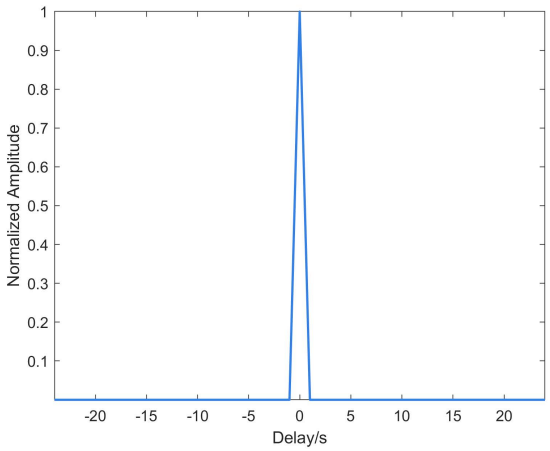

Fig. 4. Periodic ACF of P4-phase code sequence.

The autocorrelation function refers to the sum of the products of a signal with its own delayed versions at different time lags. For a discrete signal $x(n)$. Its autocorrelation function can be expressed as:

$$R_x(k) = \sum_{n=-\infty}^{\infty} x(n)x^*(n-k) \tag{4}$$

where k represents the time lag and $*$ denotes the complex conjugate operation. For a periodic signal $x(n)$ of length L, its ideal periodic autocorrelation function can be represented as:

$$c(k) = \sum_{i=1}^{L} x(i)\, x^*\left((i+k-1) \mod N+1\right), 0 \leqslant k \leqslant L-1 \tag{5}$$

where mod represents the modulo operation. Let $N = 5$, and plot the autocorrelation function of the P4 code, as shown in Fig. 4. Clearly, the autocorrelation function of the P4 code exhibits lower sidelobe levels. This is attributed to the chirp-like nature of the P4 code, where the maximum phase increment between code elements occurs at both ends of the code sequence. However, pre-compression bandwidth constraints evenly distribute the phase increments across code elements, thereby reducing the phase increment between code elements at the two ends of the P4 code sequence. This, in turn, enhances the peak-to-sidelobe ratio of the compressed pulse.

3. P4 Code Modulated OFDM Signal Model

Due to the utilization of the independence of subcarriers, parallel transmission, and frequency domain separation, there is a high degree of similarity between phase-encoded signals and OFDM signals. From a communication perspective, phase-encoded signals employ phase modulation techniques and map information onto phase states for transmission, thus bearing resemblance to MPSK modulation. For detection systems, by superimposing multiple phase-encoded signals with different frequencies in the time domain, and considering do not interfere with each other during the superposition process, resulting in a wide-spectrum OFDM phase-encoded signal [32].

According to the characteristics of P4 code, the ambiguity function of an OFDM signal can be transformed into high-resolution spectral analysis, resulting in clearer spectra for each subcarrier and reduced mutual interference between subcarriers. When performing a time-domain shift on the P4 code signal, its frequency spectrum characteristics remain unchanged, and the characteristics of its ambiguity function can still be preserved. Even in high-speed mobile environments, P4 code maintains good demodulation performance and can resist Doppler effects. In the autocorrelation function, there are distinct peaks between the P4 coding sequence and its delayed versions, which helps improve signal detection and synchronization performance. Therefore, it possesses good autocorrelation characteristics [33].

3.1 All Cyclic Shifts of P4

From the previous section, it can be observed that the P4 signal exhibits the ideal characteristics of a periodic autocorrelation function, specifically, zero sidelobes in the autocorrelation at zero period. Based on the inference drawn from LFM pulse transmission, the same phase sequence can be repeated across all subcarriers. However, introducing cyclic shifts to the phase-encoded signal adds additional degree of freedom. According to the research presented in [34], any set of ideal periodic autocorrelation sequences with different cyclic shifts forms a complementary set.

For a complex sequence X_i, where its k-th element is denoted as $s(k)$, and sum of the non-periodic autocorrelation functions R_i for all sequences in this set is denoted as $Z(p)$, $Z(p)$ equals zero for all non-zero time shifts p. This formation of a complementary set is expressed as:

$$Z(p) = \sum_{i=0}^{M-1} \sum_{k=0}^{M-1-p} s_i(k)\, s_i^*(k+p) = \begin{cases} \sum_{i=0}^{M-1} R_i(0), & p = 0 \\ 0, & p \neq 1 \end{cases} \tag{6}$$

where $*$ denotes complex conjugate, p represents a positive time shift, and $R_i(0)$ represents the energy of the sequence X_i. If the set consists of only two sequences, and these two sequences form a complementary pair, the property of complementary pairs requires that the sum of their non-periodic autocorrelation function is zero for all non-zero-time shifts. If these two sequences have periodic autocorrelation functions will not be zero, thus failing to satisfy the definition of a complementary pair. Therefore, these two complementary sequences of length M must have non-periodic autocorrelation functions. Although the magnitudes of their sidelobes are equal, their signs are opposite. The sum of these two autocorrelation functions has a peak value of $2M$ and sidelobes equal to zero.

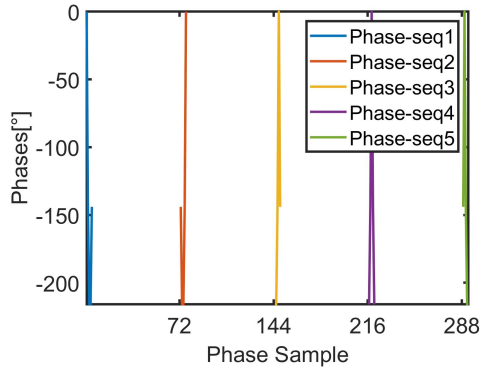

Fig. 5. Spacing between P4 complementary codes.

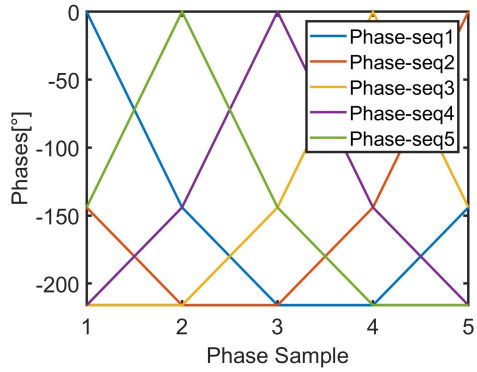

Fig. 6. Complementary set of P4 codes.

As shown in Figs. 5 and 6, a zero matrix of size $N \times N$ is created, and the formula (3) is used to generate the P4 code. The generated P4 code is then iteratively assigned to the previously created zero matrix to calculate the complementary code set and code spacing of the P4 code. When plotting the complementary code set image, the phase angle value of each complementary code sequence is added to its corresponding code spacing and multiplied by the sample position points in the code sequence to achieve the presentation of code spacing. This approach enables better demonstration of experimental data on the code spacing and orthogonality of the complementary code set of the P4 code.

From the autocorrelation function plot of the complementary code set of the P4 code sequence, as depicted in Fig. 7, it is evident that the P4 code sequence's complementary code set exhibits an ideal non-periodic autocorrelation function with zero sidelobes and complete cycle shifting. This result confirms that the P4 phase code sequence functions as an orthogonal code, where its non-periodic autocorrelation function is zero for non-zero-time delays and only takes a non-zero value at zero-time delay. This property imparts excellent complementary matching and interference resilience to the P4 phase code sequence in digital communications. Therefore, good autocorrelation performance is crucial for detecting and integrating echo signals in communication. It enhances system performance, and reliability, and enables efficient signal processing and communication functionality [35], [36].

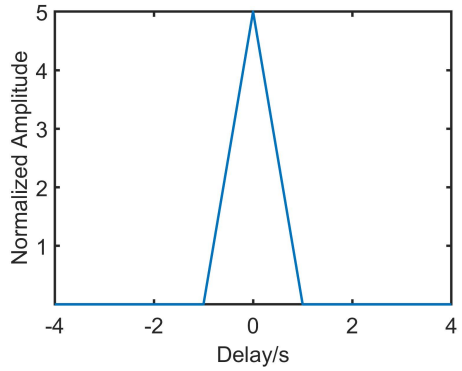

Fig. 7. Complementary set of P4 codes.

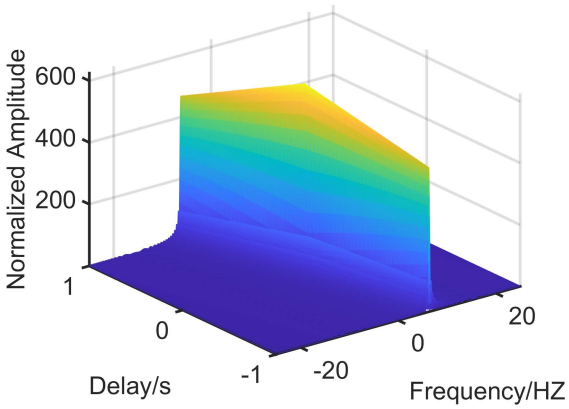

Fig. 8. Ambiguity function of conventional code.

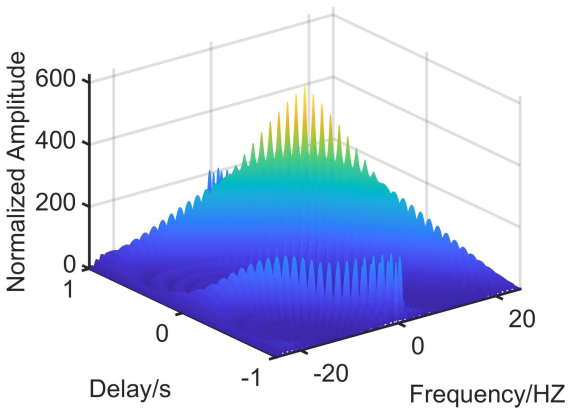

Fig. 9. Ambiguity function of P4-phase code.

3.2 P4 Code Ambiguity Function

The traditional ambiguity functions of coding waveforms, as shown in Fig. 5, compared with the P4 coding ambiguity function in Fig. 8, indicate that the P4 coding ambiguity function exhibits a multi-lobed shape, with the majority of the ambiguity volume concentrated at the ends of the coding. Moreover, Figure 9 depicts the ambiguity function of the P4 pulse with 25 elements, which exhibits a typical ridge-like pattern similar to the conventional LFM ambiguity function but with noticeable distinctions. Since both narrow

and wide pulses are primarily concentrated in the high-energy region of the ambiguity function, precise measurement and resolution of target distance can be achieved by observing the position of the narrow pulse on the frequency axis, thus achieving good distance resolution. The wide pulse exhibits a certain broadening effect along the time-delay axis, and accurate measurement and resolution of target velocity can be achieved by observing the variation in the position of the wide pulse on the time-delay axis, thereby achieving good velocity resolution.

4. MCPC Utilizing All Cyclic Shifts of P4

By analyzing the autocorrelation properties of signals [37], it is observed that when time interval between pulses is large, i.e., the pulse spacing is longer, the Doppler frequency domain has a more significant impact on phase shift. Even if the Doppler frequency shift is small, it can still result in an increase in phase shift, causing the sequence to rapidly lose the characteristic of sidelobe cancellation through autocorrelation. Therefore, it becomes necessary to use different pulses for temporal separation. This ensures that even in the presence of Doppler frequency shift, the phase shift variations between different pulses remain relatively small, thereby preserving the sequence's autocorrelation sidelobe cancellation characteristics.

On the other hand, when utilizing multiple carriers, the signal is divided into several sub-signals, each using a different carrier frequency. By modulating different frequencies, it becomes possible to separate these sub-signals at the receiving end through frequency demodulation. This theoretical possibility of signal separation is provided by employing multiple carriers.

To effectively study the properties of such signals, a redefined length of the complementary phase sequence is utilized to generate an ideal periodic autocorrelation sequence of length $M = 5$, as described in (3). Subsequently, by performing cyclic shifts, complementary codes as generated for each element and added to a zero matrix to ensure symmetry. This process ultimately yields a complementary phase sequence of length M, as depicted in Tab. 1. The five shifts of the P4 signal form a simple set of complementary codes, as indicated in the first row of Tab. 1, while the remaining entries can be viewed as all the remaining cyclic shifts.

According to the OFDM technique, we first consider the time-domain representation of the baseband signal $u_{n,m}$ for each subcarrier, where n represents the n-th subcarrier and m represents the m-th symbol. Let's assume that baseband signal has a duration of t_b. Next, we determine the frequency and phase for each subcarrier. In the frequency domain, the subcarriers are by f_s, where $f_\mathrm{s} = 1/t_\mathrm{b}$. Hence, the frequency of the n-th subcarrier can be expressed as: $2\pi t f_\mathrm{s}\left(\frac{M+1}{2} - n\right)$, where t is a time variable. Furthermore, we introduce the amplitude weight W_n and an arbitrary phase shift θ for each subcarrier. Therefore, the complex envelope of the n-th subcarrier can be represented as:

$$W_n \exp\left\{\mathrm{j}\left[2\pi t f_\mathrm{s}\left(\frac{M+1}{2} - n\right) + \theta_n\right]\right\}. \tag{7}$$

Now, convolve each subcarrier's complex envelope with the corresponding baseband signal. Since the duration of each symbol is t_b, we need to right-shift the baseband signal by $(m-1)\,t_\mathrm{b}$ to align it with the correct time point. Consequently, the signal on the n-th subcarrier can be expressed as: $u_{n,m}\left[t - (m-1)\,t_\mathrm{b}\right]$. Finally, sum up the signals from all subcarriers to obtain the mathematical expression for the complex envelope of the MCPC signal [38]:

$$u(t) = \begin{cases} \sum_{n=1}^{M} W_n \exp\left\{\mathrm{j}\left[2\pi t f_\mathrm{s}\left(\frac{M+1}{2} - n\right) + \theta_n\right]\right\} & \\ \sum_{m=1}^{M} u_{n,m}\left[t - (m-1)\,t_\mathrm{b}\right], & 0 \leqslant t \leqslant M t_\mathrm{b} \\ 0, & \text{otherwise} \end{cases} \tag{8}$$

where $u_{n,m}(t) = \begin{cases} \exp\left(\mathrm{j}\phi_{n,m}\right), & 0 \leqslant t \leqslant t_\mathrm{b} \\ 0, & \text{elsewhere} \end{cases}$ and $\phi_{n,m}$ represents the m-th symbol element of the n-th sequence.

By setting parameters such as time gap, sampling frequency, sampling rate, and number of sampling points, the waveform matrix of the pulse compression sequence is first initialized. Modulation is performed using the P4 phase sequence from the generated complementary code set, and the waveform matrix of the pulse compression sequence serves as the input. The OFDM system is used to generate the final signal waveform, as shown in Fig. 10.

From previous figures, it can be observed the typical P4 pulse exhibits an ideal autocorrelation with a narrow main lobe and zero sidelobes. In the designed new waveform, the waveform graph shows the modulation of N subcarriers with a sequence *length* = 5, and the time gap t_b for each sequence is chosen as N times the sampling time t_c of each phase. This will result in autocorrelation as shown in Fig. 11, similar to the P4 pulse in terms of autocorrelation main lobe width. By calculation, the main lobe width is determined to be 1.39 dB, and the sidelobe level is 0.21 dB. A narrower main lobe implies higher resolution in the time domain, enabling accurate determination of signal arrival time or position. A lower sidelobe level indicates that the amplitude of the autocorrelation function outside the main lobe region is small, reducing the energy of the autocorrelation function outside the main lobe, thereby minimizing the influence of interference or noise.

Seq. 1	Seq. 2	Seq. 3	Seq. 4	Seq. 5
0°	−144°	−216°	−216°	−144°
−144°	−216°	−216°	−144°	0°
−216°	−216°	−144°	0°	−144°
−216°	−144°	0°	−144°	−216°
−144°	0°	−144°	−216°	−216°

Tab. 1. Set of five complementary phase coded sequences.

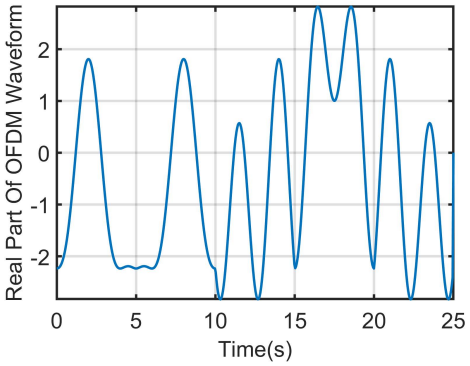

Fig. 10. P4-OFDM waveform of *Length* = 5.

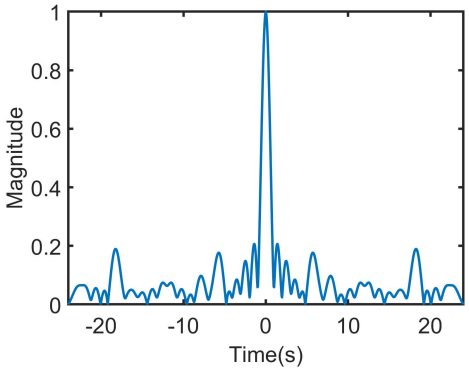

Fig. 11. P4-OFDM autocorrelation.

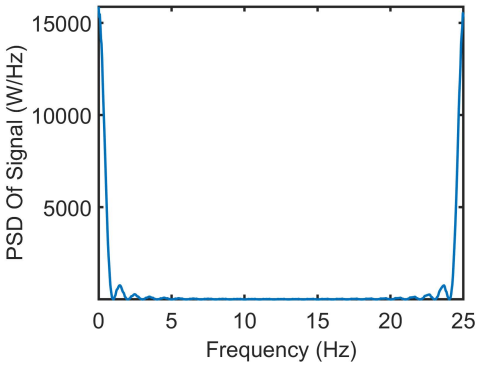

Fig. 12. PSD of P4-OFDM waveform.

In general, based on its autocorrelation function, it can be observed that the addition of P4 phase coding results in a significantly low sidelobe level in P4-OFDM signals. Therefore, it can enhance the peak sidelobe ratio of MCPC radar signals and further improve the signal power utilization efficiency.

Due to the lower level of the autocorrelation function, the waveform's autocorrelation can better maintain high autocorrelation even in the presence of interference signals or noise, thereby improving the system's anti-interference capability and enabling the receiver to more accurately extract the desired signal. Furthermore, the more efficient spectral utilization of MCPC pulses will be demonstrated, as shown in Fig. 12, where the power spectrum approximates as rectangular shape with a cutoff time of $f \approx M/2t_b$.

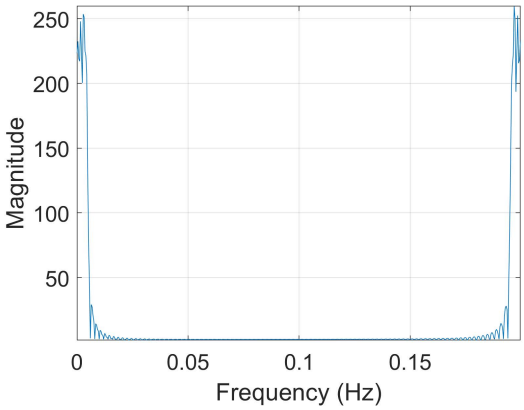

Fig. 13. Frequency spectrum characteristics of P4-OFDM waveform.

The ambiguity function of $u(t)$ and its zero Doppler intercept, which represents the amplitude of autocorrelation, depend on the arrangement of 5 sequences along 5 subcarriers $(2f_s, f_s, 0, -f_s, -2f_s)$. In other words, by using 5 subcarriers, we create an autocorrelation similar to a single-frequency signal with 5 times the number of bits within the same total duration. It is worth noting the presence of null values in the autocorrelation function at multiples of t_b. These null values are generated by the combination of orthogonality $(f_s = 1/t_b)$ and complementary sets. The phase sequences of the P4 signal with 25 elements utilize 13 different phase value, in comparison to only three different values in Tab 1. Additionally, the occupied spectrum and Doppler sensitivity need to be compared. Figure 13 demonstrates the frequency spectrum characteristics corresponding to MCPC pulses, obtained by using the waveform matrix of the pulse compression sequence as the output and applying a FFT using the OFDM system to generate the final signal waveform. Generally, MCPC signals exhibit narrow and flatter spectra (complex envelopes) extending up to $f_{max} \approx M/2t_b$. Therefore, near the center frequency, the bandwidth of a passband signal can be represented as:

$$BW = 2f_{max} \approx M/t_b. \tag{9}$$

The ambiguity function, as illustrated in Fig. 14, are compared with those in Fig. 9. These two figures represent the ambiguity functions of P4-OFDM signals utilizing non-cyclically shifted P4 codes and cyclically shifted P4 codes, respectively. It is evident that the performance of the ambiguity function of P4-OFDM signals, after applying cyclic shifting, surpasses that of non-cyclically shifted ones. This enhancement contributes to mitigating the 'slant-tough' shape observed in the blur function of non-cyclically shifted P4-OFDM signals. Furthermore, when compared to the typical LFM signal's ambiguity function, there is no pronounced ridge structure in the ambiguity function of cyclically shifted P4-OFDM signals. Consequently, this improvement enhances the radar detection capability.

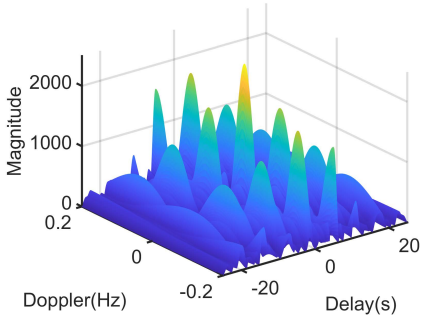

Fig. 14. Ambiguity function of P4-OFDM waveform.

5. Numerical Analysis of a Train of Complementary MCPC Pulses

5.1 PMEPR Comparison in MCPC for Various Orders

Due to phase differences between subcarriers, different modulation schemes, and Doppler frequency shifts, MCPC signals are susceptible to envelope variations. To maintain power amplifier linearity, meet signal bandwidth requirements, and avoid exceeding power supply limitations, it is necessary to reduce the PMEPR in the signal generator with power amplifiers. This helps improve signal quality and reliability, ensuring the normal operation of the system under different power requirements. The orthogonality of MCPC signals means that subcarriers are mutually independent and free from interference during the duration, enhancing resistance to multipath fading and increasing system capacity. Therefore, within a bit duration, assuming each subcarrier has unit power, the power of individual subcarriers may simultaneously reach their peaks. As a result, a maximum of M subcarriers can reach their peals simultaneously, leading to an instantaneous peak power of up to M^2. Ultimately, the following conclusion can be drawn:

$$PMEPR \leqslant M. \tag{10}$$

Assuming an $M > 4$ P4 sequence is $\{1, 2, 3, 4, 5\}$, during the cyclic shift, each element is moved one position to the right or left according to the order in the sequence, and the last element is placed at the beginning of the sequence. This process generates new sequences such as $\{5, 1, 2, 3, 4\}$, $\{4, 5, 1, 2, 3\}$, and so on. By using this cyclic shift-based approach of the original P4 sequence. This method can be extended as follows:

$$\begin{aligned} &\{k, k+1, \cdots, M-1, M, 1, 2, \cdots, k-1\}, \\ &\{k, k-1, \cdots, 2, 1, M, M-1, \cdots, k+1\}. \end{aligned} \tag{11}$$

It is important to note that Boyd has indicated the result in (10), namely:

$$PMEPR \leqslant 2.015. \tag{12}$$

By applying (11) for the optimal sequence permutation of subcarriers to reduce sidelobes, Figure 15 illustrates the real envelope plots of 5×5 MCPC signals based on P4 with sequence order $\{1, 2, 3, 4, 5\}$ and $\{3, 5, 2, 1, 4\}$. The latter satisfies the condition defined by Boyd in (12). The corresponding PMEPR values are 4.4073 and 1.7371, respectively. For convenient comparison, Figure 16 and Figure 17 present the autocorrelation and ambiguity function plots of the optimal sequences, with corresponding PSL values of -18 dB and -13.75 dB, respectively.

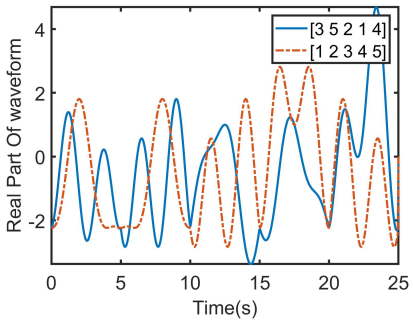

Fig. 15. MCPC waveform of ordinary and optimal sequence.

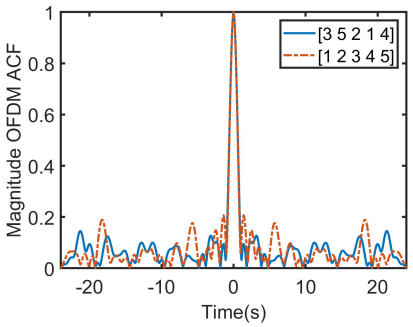

Fig. 16. ACF of OFDM waveform ordinary sequence and optimal sequence.

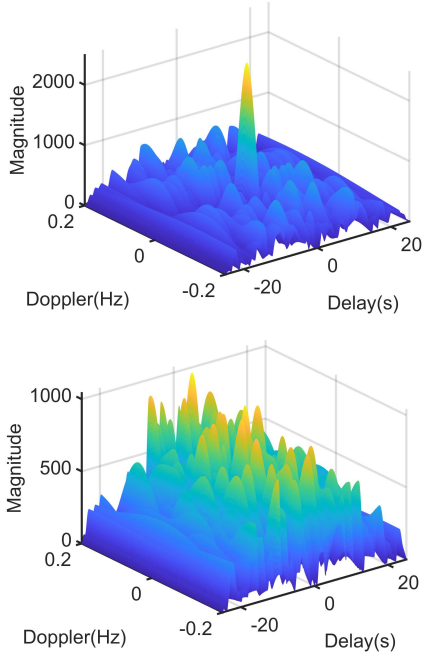

Fig. 17. The ambiguity function of MCPC waveform the ordinary sequence and optimal sequence.

5.2 Optimizing the Pulse for Signal

In this section, we will use genetic algorithm techniques to optimize the PMEPR value. The first step in implementing any genetic algorithm is to generate an initial population. Following the guidelines of genetic algorithm specification [39], this involves encoding each element of the population as a binary string. The genetic algorithm implemented in this work is a two-stage process, which is often referred to as a Simple-Genetic-Algorithm (SGA) by Goldberg [40]. Starting from the current population, an intermediate population is formed through section.

Then, the next generation is formed by recombination and mutation, representing the process from the current population to the next population in the genetic algorithm. As mentioned earlier, we apply this algorithm for single-objective PMEPR optimization. The specific process is as follows:

1. Initialize the number of subcarriers N, the number of symbols K in a pulse, the population size pop, the maximum number of iterations, the mutation rate, the duration, the duration of one symbol t_b, and the frequency spacing Δf.
2. Initialize the population by randomly generating a binary matrix of size $pop \times N$, representing the population, where each individual represents a set of subcarrier allocations.
3. Create a one-dimensional zero vector of the same size as the maximum number of iterations and initialize the best fitness plot to record the best fitness value for each generation.
4. Calculate the fitness value of each individual in the population by evaluating the oversampled complex OFDM signal, which is obtained by applying an IDFT to the phase code [41], to measure the quality of the individual's solution.
5. Calculate the PMEPR value according to (11) and associate it with the corresponding individual.
6. Select parent individuals based on their fitness values for generating the next generation.
7. Perform fixed-point crossover operations on the selected parent individuals to generate new offspring individuals.
8. Perform mutation operations on the offspring individuals by independently mutating each gene with a certain probability, introducing new gene variations.
9. Update the best individual by identifying the individual with the lowest fitness value in the current population and recoding its fitness value and gene sequence.
10. Repeat steps 3 to 9 until the maximum number of iterations is reached and converges to the optimal solution.

In the improved genetic algorithm, we aim to enhance the algorithm's performance. In the crossover operation, instead of using fixed crossover points, we randomly select crossover points for each crossover, increasing the diversity of the population. This ensures better exploration of the search space and improves the globe search capability.

In the mutation operation, we calculate the number of genes to mutate based on the population size, chromosome length, and mutation rate. Then, we randomly select these genes for mutation rate and reduces the number of ineffective mutation mutations during iteration. From Fig. 18, it can be observed that the PMEPR values obtained by optimizing with both the traditional genetic algorithm and the improved genetic algorithm are compared, and it is evident that PMEPR is significantly reduced. And the resulting waveforms are finally compared and presented together as shown in Fig. 19. This validates the feasibility of the improved genetic algorithm.

In Fig. 19, the generated complementary MCPC sequence is extended to twice the length of the original sequence, and the time axis is constrained to the pulse duration $(M^2 \times t_b)$. In this case, when the pulse period T is greater than twice the pulse width $(T > 2Mt_b)$, it implies the presence of multiple complete pulses within the time range. Due to the complementary relationship among these pulses, the autocorrelation within this delay range is not influenced by the specific value of T.

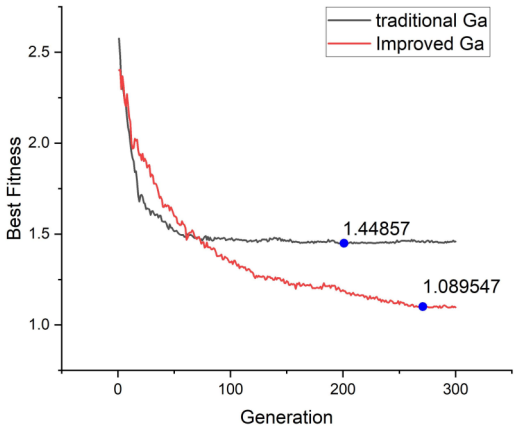

Fig. 18. Traditional Ga vs Improved Ga.

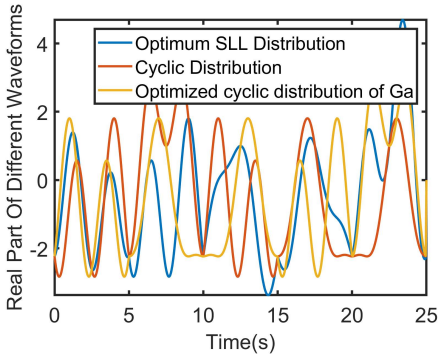

Fig. 19. Waveforms comparison between cyclic, optimum order and Ga.

5.3 Frequency Weighted Complementary MCPC Pulse

By applying frequency weighting, it is possible to effectively reduce the sidelobes in the autocorrelation of LFM radar signals and mitigate interference from other signals or noise [37]. In traditional constant-amplitude radar signals, to restore the signal's constant amplitude characteristics and compensate for amplitude variations during signal transmission, weighting is typically performed only at the receiver. However, due to the ideal nature of the matched filter, performing weighting solely at the receiver cannot completely eliminate the impact of non-ideal factors, leading to the degradation of the signal's constant amplitude characteristics. Despite the extensive knowledge of weighting window function, we confine our numerical experiments to a simple family of weighting functions expressed mathematically as:

$$W_n = \left[a_0 + a_1 \cos\left(\frac{2\pi \left(n - \frac{1}{2} \right)}{M} \right) \right]^{\alpha}. \tag{13}$$

Note that, $a_0 = 0.53826$ and $a_1 = 0.46164$ are set as the coefficients at the two endpoints of the Hamming window, and $\alpha = 0.5$ is the coefficient at the center endpoint. This is equivalent to adding a Hamming window at the receiver end. The permutation-based on MCPC sequence is then subjected to Hamming window frequency weighting to reduce sidelobes. Subsequently, the resulting complementary MCPC sequence, after being frequency-weighted with the Hamming window, is transformed into a time-domain waveform, as shown in Fig. 20.

The Kaiser window is a type of window function used in signal processing and spectrum analysis, typically employed to control spectral leakage and main lobe width. Its mathematical expression is as follows:

$$W_n = \frac{I_0 \left(\beta \sqrt{1 - \left(\frac{n-N}{N} \right)^2} \right)}{I_0 (\beta)} \tag{14}$$

where I_0 is the is the modified Bessel function of the first kind, β is the shape parameter of the window function, it is set to 5, and N is the length of the window, typically an even number. Subsequently, a Kaiser window frequency-weighting is applied to the permutation-based MCPC sequence, followed by a transformation into the time-domain waveform, as illustrated in Fig. 21.

And the mathematical expression of the Taylor window is given as follows:

$$W_n = \sum_{k=0}^{M} \frac{(-1)^k}{k!} \left(\frac{2n}{N} - 1 \right)^k \tag{15}$$

where M represents the order of the Taylor window, which determines the shape of the window, and for the sake of comparison, we have also set it to 5. Subsequently, a Taylor window frequency-weighting is applied to the permutation-based MCPC sequence, followed by a transformation into the time-domain waveform, as illustrated in Fig. 22.

Next, the ACF of the complementary MCPC time-domain waveform with Hamming window frequency weighting is computed. The corresponding delay vector is generated based on the time vector of the complementary code, representing the correlation between the weighted ACF of the complementary MCPC sequence at different time intervals. The amplitude of the obtained ACF is shown in Fig. 23. Based on the calculations, the computed PSL value for the complementary MCPC sequence with Hamming window frequency weighting is −30.17 dB. Similarly, the ACF weighted by the Kaiser window and the Taylor window are depicted in Figs. 24 and 25, respectively. These two plots exhibit subtle differences.

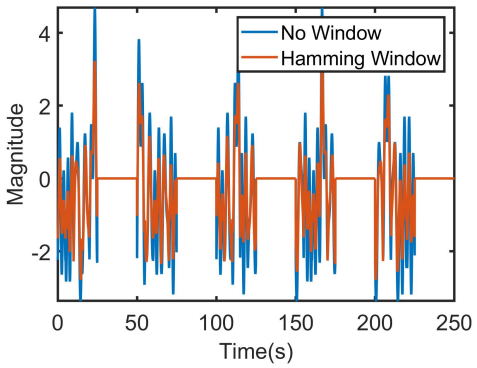

Fig. 20. Real part of train of complementary MCPC waveform, no Window vs Hamming Window.

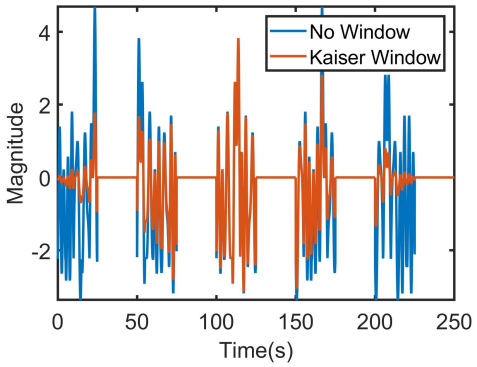

Fig. 21. Real part of train of complementary MCPC waveform, no Window vs Kaiser Window.

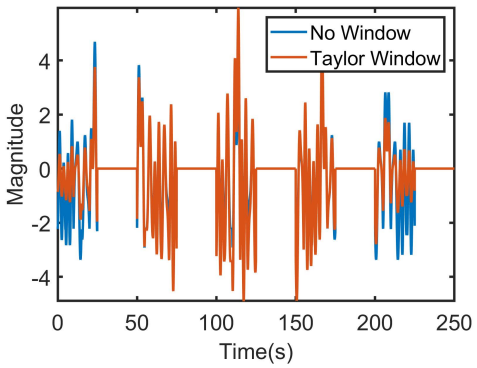

Fig. 22. Real part of train of complementary MCPC waveform, no Window vs Taylor Window.

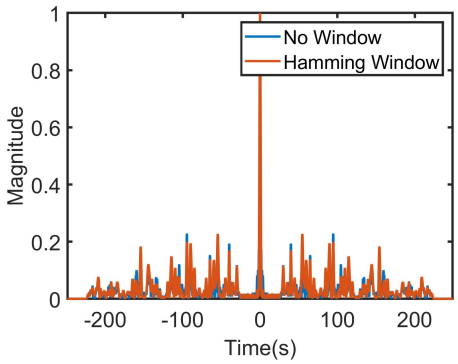

Fig. 23. Train of complementary MCPC ACF, no Window vs Hamming Window.

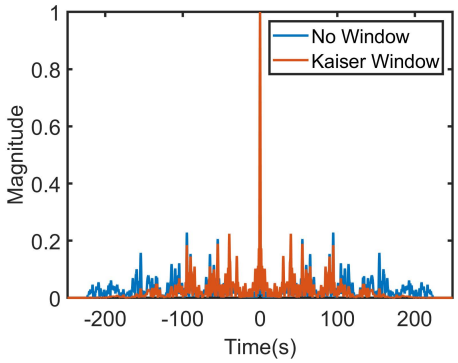

Fig. 24. Train of complementary MCPC ACF, no Window vs Kaiser Window.

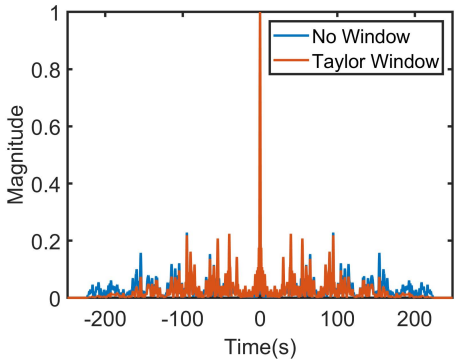

Fig. 25. Train of complementary MCPC ACF, no Window vs Taylor Window.

6. Conclusions

The MCPC signal offers several advantages over known signals. By optimizing subcarrier sequence permutations, the MCPC signal achieves a significant reduction in sidelobes and PMEPR value, resulting in a smaller peak power. This addresses the issue of insufficient dynamic range during transmission, allowing the radar system to handle the dynamic range difference between strong and weak targets effectively. MCPC, similar to the P4 signal, is a digital phase modulation signal but with more phase states and frequency selections. It possesses a pin-like ambiguity function and requires fewer phase values.

Despite being essentially a pulse signal, MCPC inherits favorable aperiodic autocorrelation characteristics from the periodic autocorrelation of its underlying signal. This allows the design and analysis of MCPC signals to draw knowledge from signals with complete periodic autocorrelation, achieving improved aperiodic autocorrelation characteristics and performance. As a multi-frequency signal, MCPC benefits from frequency weighting, which reduces autocorrelation sidelobes. Designing complementary states along each pulse and frequency using MCPC pulse trains further reduces sidelobes.

Lastly, for an $M \times M$ MCPC signal, there are $M!$ (factorial of M) different permutations. Among all possible sequences, an optimal sequence can be found, exhibiting relatively lower peak values in the ambiguity function. This can reduce mutual interference among nearby radar instruments.

In conclusion, the analysis of MCPC radar signal characteristics underscores their significance in both MIMO radar systems and radar-communication integration. Signals with a low PMEPR are instrumental in reducing interference and improving the dynamic range, thereby enhancing the effectiveness of MIMO radar for target detection and tracking. Additionally, the strong autocorrelation of MCPC signals, indicative of high temporal and spectral correlation, enhances signal distinctiveness and resolution within MIMO radar systems, enabling precise differentiation of multiple targets and the provision of accurate positional information. Furthermore, MCPC radar signals, with their spectral versatility, allow for information distribution across multiple subcarriers, facilitating simultaneous radar and data communication in the same frequency band, without the need for additional spectrum allocation. The low PMEPR of MCPC signals ensures stable data communication, enabling the system to perform consistently across diverse operational requirements in radar-communication integration.

Acknowledgments

This research has been supported by the National Natural Science Foundation of China (No. 61801412) and Technology Program of Fujian Province (No. 2020J01298). The authors express their gratitude to the valuable feedback provided by the reviewers.

References

[1] LARSSON, E. G., EDFORS, O., TUFVESSON, F., et al. Massive MIMO for next generation wireless systems. *IEEE Communications Magazine*, 2014, vol. 52, no. 2, p. 186–195. DOI: 10.1109/MCOM.2014.6736761

[2] STURM, C., ZWICK, T., WIESBECK, W., et al. An OFDM system concept for joint radar and communications operations. In *VTC Spring 2009 - IEEE 69th Vehicular Technology Conference*. Barcelona (Spain), 2013, p. 1–5. DOI: 10.1109/VETECS.2009.5073387

[3] CHENG, S. J., WANG, W. Q., SHAO, H. Z., et al. Spread spectrum-coded OFDM chirp waveform diversity design. *IEEE Sensors Journal*, 2015, vol. 15, no. 10, p. 5694–5700. DOI: 10.1109/JSEN.2015.2448617

[4] TIAN, X., SONG, Z. On radar and communication integrated system using OFDM signal. In *IEEE Radar Conference (RadarConf)*. Seattle (USA), 2017, p. 318–0323. DOI: 10.1109/RADAR.2017.7944220

[5] LI, C., BAO, W., XU, L., et al. Radar communication integrated waveform design based on OFDM and circular shift sequence. *Mathematical Problems in Engineering*, 2017, vol. 2017, p. 1–10. DOI: 10.1155/2017/9840172

[6] ELLINGER, J., ZHANG, Z., WICKS, M., et al. Multi-carrier radar waveforms for communications and detection. *IET Radar, Sonar & Navigation*, 2017, vol. 11, no. 3, p. 444–452. DOI: 10.1049/iet-rsn.2016.0244

[7] LEVANON, N. Multifrequency radar signals. In *Record of the IEEE International Radar Conference [Cat. No. 00CH37037]*. Alexandria (USA), 2000, p. 683–688. DOI: 10.1109/RADAR.2000.851916

[8] LEVANON, N., MOZESON, E. Multicarrier radar signal-pulse train and CW. *IEEE Transactions on Aerospace and Electronic Systems*, 2002, vol. 38, no. 2, p. 707–720. DOI: 10.1109/TAES.2002.1009000

[9] MOZESON, E., LEVANON, N. Multicarrier radar signals with low peak-to-mean envelope power ratio. *IEE Proceedings-Radar, Sonar and Navigation*, 2003, vol. 150, no. 2, p. 71–77. DOI: 10.1049/ip-rsn:20030263

[10] DENG, B., SUN, B., WEI, X., et al. Ambiguity function analysis for MCPC radar signal. In *International Conference on Industrial Mechatronics and Automation*. Wuhan (China), 2010, p. 650–653. DOI: 10.1109/ICINDMA.2010.5538224

[11] FARNANE, K., MINAOUI, K., ROUIJEL, A., et al. Analysis of the ambiguity function for phase-coded waveforms. In *IEEE/ACS 12th International Conference of Computer Systems and Applications (AICCSA)*. Marrakech (Morocco), 2015, p. 1–4. DOI: 10.1109/AICCSA.2015.7507195

[12] RIHACZEK, A. W. *Principles of High-Resolution Radar*. McGraw-Hill Book Company, 1969. ISBN: 0754321069

[13] KAYVAN, R. *Radar Signals*. Press Institute of Imam Hussein University, 2023. ISBN: 9786222860905

[14] LEVANON, N. *Radar Principles*. Wiley, 1988. ISBN: 9780471858812

[15] MAHAFZA, B. R. *Radar Systems Analysis and Design Using MATLAB*. Chapman and Hall/CRC, 2022. ISBN: 9780367507930

[16] LEVANON, N. Stepped-frequency pulse-train radar signal. *IEE Proceedings-Radar, Sonar and Navigation*, 2003, vol. 149, no. 6, p. 297–309. DOI: 10.1049/ip-rsn:20020432

[17] GOLOMB, S. W., TAYLOR, H. Constructions and properties of Costas arrays. *Proceedings of the IEEE*, 1984, vol. 72, no. 9, p. 1143–1163. DOI: 10.1109/PROC.1984.12994

[18] LEVANON, N., MOZESON, E. Nullifying ACF grating lobes in stepped-frequency train of LFM pulses. *IEEE Transactions on Aerospace and Electronic Systems*, 2003, vol. 39, no. 2, p. 694–703. DOI: 10.1109/TAES.2003.1207275

[19] SHARMA, S., BICÁ, M., KOIVUNEN, V. Reduced PMEPR multicarrier radar waveform design. In *53rd Asilomar Conference on Signals, Systems, and Computers*. Pacific Grove (USA), 2019, p. 2048–2052. DOI: 10.1109/IEEECONF44664.2019.9048815

[20] MOHSENI, R., SHEIKHI, A., SHIRAZI, M. A. M. Compression of multicarrier phase-coded radar signals with low sampling rate. In *International Conference on Radar*. Adelaide (Australia), 2008, p. 718–721. DOI: 10.1109/RADAR.2008.4654014

[21] MOHSENI, R., SHEIKHI, A., SHIRAZI, M. A. M. A new approach to compress multicarrier phase-coded signals. In *IEEE Radar Conference*. Rome (Italy), 2008, p. 1–6. DOI: 10.1109/RADAR.2008.4720800

[22] LI, J., ZHOU, J., WANG, W., et al. A radar waveform design of MCPC method for interrupted sampling repeater jamming suppression via fractional Fourier transform. *Progress In Electromagnetics Research C*, 2023, vol. 129, p. 1–15. DOI: 10.2528/PIERC22102001

[23] BICÁ, M., KOIVUNEN, V. Multicarrier radar-communications waveform design for RF convergence and coexistence. In *IEEE International Conference on Acoustics, Speech and Signal Processing (ICASSP)*. Brighton (UK), 2019, p. 7780–7784. DOI: 10.1109/ICASSP.2019.8683655

[24] BICÁ, M., KOIVUNEN, V. Generalized multicarrier radar: Models and performance. *IEEE Transactions on Signal Processing*, 2016, vol. 64, no. 17, p. 4389–4402. DOI: 10.1109/TSP.2016.2566610

[25] HASSAN, W. Textile dual band antenna printed on artificial heart bag for WBAN communications. *Progress In Electromagnetics Research C*, 2023, vol. 129, p. 273–287. DOI: 10.2528/PIERC23010904

[26] DONNET, B. J., LONGSTAFF, I. D. Combining MIMO radar with OFDM communications. In *IEEE European Radar Conference (EURAD)*. Manchester (UK), 2006, p. 37–40. DOI: 10.1109/EURAD.2006.280267

[27] LELLOUCH, G., NIKOOKAR, H. On the capability of a radar network to support communications. In *14th IEEE Symposium on Communications and Vehicular Technology in the Benelux (SCVT)*. Delft (Netherlands), 2007, p. 1–5. DOI: 10.1109/SCVT.2007.4436249

[28] GARMATYUK, D., SCHUERGER, J., MORTON, Y. T., et al. Feasibility study of a multi-carrier dual-use imaging radar and communication system. In *IEEE European Microwave Conference (EURAD)*. Munich (Germany), 2007, p. 1473–1476. DOI: 10.1109/EURAD.2007.4404970

[29] WU, K., CHU, N., WU, D., et al. The Enkurgram: A characteristic frequency extraction method for fluid machinery based on multi-band demodulation strategy. *Mechanical Systems and Signal Processing*, 2021, vol. 155, p. 1–34. DOI: 10.1016/j.ymssp.2020.107564

[30] LIU, Z., ZHANG, Y., LUO, X. Performance analysis of radar communication shared signal based on OFDM. In Gao, H., Wun, J., Yin, J., et al. (eds.) *Communications and Networking. ChinaCom 2021. Lecture Notes of the Institute for Computer Sciences, Social Informatics and Telecommunications Engineering*, 2022, vol. 433, p. 250–263. DOI: 10.1007/978-3-030-99200-2_20

[31] MURALIDHARA, N., VINOD, V., SANTHOSHKUMAR, D., et al. Comparative analysis of polyphase codes for digital pulse compression applications. *International Journal of Engineering Research & Technology*, 2014, vol. 3, no. 10, p. 1–5. DOI: 10.17577/IJERTV3IS100764

[32] MOHSENI, R. SHEIKHI, A., MASNADI-SHIRAZI, M. A. Multicarrier constant envelope OFDM signal design for radar applications. *AEU-International Journal of Electronics and Communications*, 2010, vol. 64, no. 11, p. 999–1008. DOI: 10.1016/j.aeue.2009.10.008

[33] XIAO, Z., ZENG, Y. Waveform design and performance analysis for full-duplex integrated sensing and communication. *IEEE Journal on Selected Areas in Communications*, 2022, vol. 40, no. 6, p. 1823–1837. DOI: 10.1109/JSAC.2022.3155509

[34] POPOVIĆ, B. M. Complementary sets based on sequences with ideal periodic autocorrelation. *Electronics Letters*, 1990, vol. 26, no. 18, p. 1428–1430. DOI: 10.1049/el:19900916

[35] KOOPMAN, P. 32-bit cyclic redundancy codes for internet applications. In *Proceedings International Conference on Dependable Systems and Networks*. Washington (USA), 2002, p. 459–468. DOI: 10.1109/DSN.2002.1028931

[36] INDUMATHI, G., ANANTHAKIRUPA, V. A. A., RAMESH, M. Architectural design of 32 bit polar encoder. *Circuits and Systems*, 2016, vol. 7, no. 5, p. 1–11. DOI: 10.4236/cs.2016.75047

[37] FARNETT, E. C., STEVENS, G. H., SKOLNIK, M. Pulse compression radar. Chapter in Skolnik, M. I. *Radar Handbook 2*, 1990, p. 10–11. ISBN: 007057913X

[38] LEVANON, N. Multifrequency complementary phase-coded radar signal. *IEE Proceedings-Radar, Sonar and Navigation*, 2000, vol. 147, no. 6, p. 276–284. DOI: 10.1049/ip-rsn:20000734

[39] MIRJALILI, S. *Evolutionary Algorithms and Neural Networks: Theory and Applications*. Heidelburg (Australia): Springer International Publishing, 2019. ISBN: 9783030065720

[40] WHITLEY, D. A genetic algorithm tutorial. *Statistics and Computing*, 1994, vol. 4, p. 65–85. DOI: 10.1007/BF00175354

[41] LELLOUCH, G., TRAN, P., PRIBIC, R., et al. OFDM waveforms for frequency agility and opportunities for Doppler processing in radar. In *IEEE Radar Conference*. Rome (Italy), 2008, p. 1–6. DOI: 10.1109/RADAR.2008.4720798

About the Authors ...

Doudou HUANG was born in Yichun Jiangxi. He received his B.E. degree from Qindao College of Qingdao Technological University, P.R. China in 2017. He is currently pursuing the M.E. degree at Electronic Information, Xiamen University of Technology, P.R. China. His research interests include radar waveform design on optimization theory.

Jun TANG (corresponding author) received his M.S. and Ph.D. degrees in Information and Communication Engineering form Xidian University and Xiamen University, China, in 2007 and 2008, respectively. He is currently an Associate Professor in the Department of Communication Engineering, Xiamen University of Technology. His major research interests include image processing, radar signal processing, and multimedia signal processing.

Longshan XU (corresponding author) received his M.S. and Ph.D. degrees in Materials Science and Engineering from Hunan University, China, in 2007 and 2009, respectively. He is currently an Associate Professor in the Department of Materials Science and Engineering, Xiamen University of Technology. His major research interests include copper base electrical contact material.

Yurong WU received her M.S. and Ph.D. degrees in Materials Science and Engineering from Hunan University, China, in 2007 and 2009, respectively. She is currently an Associate Professor in the Department of Materials Science and Engineering, Xiamen University of Technology. Her major research interests include metal oxide catalytic energy storage materials.